Voronoi space division of a polymer: Topological effects, free volume, and surface end segregation

AUTHOR(S):

Tokita, N; Hirabayashi, M; Azuma, C; Dotera, T

CITATION:

Tokita, N ...[et al]. Voronoi space division of a polymer: Topological effects, free volume, and surface end segregation. JOURNAL OF CHEMICAL PHYSICS 2004, 120(1): 496-505

ISSUE DATE:

2004-01-01

URL:

http://hdl.handle.net/2433/50199

JOURNAL OF CHEMICAL PHYSICS VOLUME 120, NUMBER 1 1 JANUARY 2004

Voronoi space division of a polymer: Topological effects, free volume, and surface end segregation

Nakako Tokita and Megumi Hirabayashi
Saitama Study Center, the University of the Air, Saitama 331-0851, Japan

Chiaki Azuma
Setagaya Study Center, the University of the Air, Tokyo 154-0002, Japan

Tomonari Dotera[a)]
Department of Polymer Chemistry, Graduate School of Engineering, Kyoto University, Kyoto Daigaku Katsura, Kyoto 615-8510, Japan

(Received 7 August 2003; accepted 3 October 2003)

In order to investigate the topological effects of chain molecules, united-atom molecular dynamics simulations of a 500-mer polyethylene linked by 50 hexyl groups (a grafted polymer having 52 ends) are carried out and analyzed in terms of Voronoi space division. We find that the volume of a Voronoi polyhedron for a chain end is larger than that for an internal or junction atom, and that it is the most sensitive to temperature, both of which suggest higher mobility of chain ends. Moreover, chain ends dominantly localize at the surface of the globule: The striking evidence is that while the ratio of surface atoms is only 24% of all atoms, the ratio of ends at the surface is 91% out of all ends. The shape of Voronoi polyhedra for internal atoms is prolate even in the bulk, and near the surface it becomes more prolate. We propose the concept of *bonding faces*, which play a significant role in the Voronoi space division of covalently bonding polymers. Two bonding faces occupy 38% of the total surface area of a Voronoi polyhedron and determine the prolate shape. © *2004 American Institute of Physics.* [DOI: 10.1063/1.1629678]

I. INTRODUCTION

Voronoi analysis has been applied to study simple liquids and noncrystalline metallic solids to characterize the distributions of atoms.[1–7] It consists of partitioning a space into a set of polyhedra and analyzing their volume and shape. In polymer science, the analysis has been used for bulk[8] and isolated[9] polymer chains. A fundamental question arises concerning the volume and shape of Voronoi polyhedra: In contrast to simple liquids or metallic glasses, are there any specific features of polymers?; Does chain connectivity have an influence upon the volume and the shape of Voronoi polyhedra? In this article, we show that the existence of bonds definitely affects Voronoi space division.

Here, we deal with a simplified simulational polymer model called the *united-atom model*, in which an atom represents one of CH_3, CH_2, and CH groups. Hydrogens are not explicitly modeled as distinct atoms, and an atom signifies one of the united atoms hereafter. A chain is thus represented by united atoms and bonds between neighboring united atoms. In the present study a model chain is a 500-mer polyethylene linked by 50 hexyl groups ($-C_6H_{13}$) per 10 repeating units as side chains (Fig. 1). Notice that in the united-atom scheme, there are three kinds of topologically different atoms with respect to the number of bonds: *end* atoms with one bond, *internal* atoms with two bonds, and *junction* atoms with three bonds. We will show that the number of bonds from an atom has a great influence on the volume of a Voronoi polyhedron and its temperature dependence. Our concern is the space partitioning of the united atoms of three types and the term *topological effect* here renders the effect of the number of bonds.

The so-called free volume argument relates to the topological effect. More than five decades ago, Fox and Flory[10] found that the specific volume and the glass transition temperature (T_g) of polystyrene depend on the molecular weight (M_n) as a linear function of M_n^{-1}, and they explained that the phenomena are caused by the larger free volume of end groups; the number density of end groups is proportional to M_n^{-1}. In this direction, Rigby and Roe[8] have shown in their simulation of amorphous polymers that the volume of a Voronoi polyhedron containing an end is much larger than that containing an internal atom.

Furthermore, the Volonoi analysis is not only applicable to bulk, but also to surfaces. Soyer *et al.*[9] recently reported a Voronoi analysis of packing geometry of amino acids in folded proteins, and used the method to distinguish the bulk and the surface. We also use the method to distinguish the bulk and the surface of our chain and find that end groups segregate at the surface, implying that the topological effect appears at the surface as well.

Though our model is just an isolated chain in a vacuum, this end segregation effect reminds us of recent studies on surfaces of bulk polymers. The dependence of surface tension upon M_n^{-1} has been interpreted on one hand by the free volume argument of chain ends,[11,12] and on the other hand, by the end segregation effect to reduce conformational en-

[a)]Author to whom correspondence should be addressed. Electronic mail: dotera@phys.polym.kyoto-u.ac.jp

FIG. 1. Schematic sketch of the model molecule, $[(\text{-}CH_2CH_2\text{-})_4(\text{-}CH_2CH(C_6H_{13})\text{-})(\text{-}CH_2CH_2\text{-})_5]_{50}$. The main chain is 500-mer polyethylene. The number of ends is 52.

tropy loss.[13,14] A number of theoretical studies on the surface end segregation has appeared,[15–23] and experimental evidence of the surface end segregation has been reported in the study of mainly end-labeled polystyrene.[24–27] On this line, a depression of the surface T_g compared with that for amorphous polymer bulk is theoretically predicted[22] and experimentally confirmed.[28]

This article is organized as follows: In Sec. II, we describe our simulation method: A united-atom polymer model, the Dreiding force field, dynamics, initial conditions, and sample preparation. In Sec. III, we discuss the state of a polymer chain: The radius of gyration, asphericity, and the radial distributions of atoms. Section IV is the main part of the article. In the Sec. IV A, we describe the detailed procedure of Voronoi division. Section IV B contains the analysis of Voronoi polyhedra. The inverse volume distribution reveals the following features: (1) There are two different circumstances, i.e., surface and bulk parts in this system, (2) the volume of a polyhedron strongly depends on the number of bonds, and the averaged volume associated with ends is the largest with the greatest *local* thermal expansion coefficient, and (3) ends segregate at the surface. Section IV C is devoted to the characterization of polyhedron shapes. We introduce the concept of bonding faces and elucidate a significant role of the bonding faces. Section V is the conclusion.

II. METHOD

A. Model

The model molecule is a 500-mer polyethylene linked by 50 hexyl groups: $[(\text{-}CH_2CH_2\text{-})_4(\text{-}CH_2CH(C_6H_{13})\text{-})(\text{-}CH_2CH_2\text{-})_5]_{50}$. We choose a simple and typical polymer, polyethylene as a main chain. To gain meaningful statistics for end and junction atoms, a polymer with 50 side chains is selected with intent to increase the number of these atoms.

We note that it is hard to synthesize the periodically grafted molecules because linked segments seem to be randomly positioned, however, we presume that the main results of the article are independent of the periodicity.

B. Force field

According to the Dreiding force field (Tables I and II),[29] we employ the following energy terms for an arbitrary geometry of molecules. Valence interactions consist of bond stretching (E_b), bond angle bending (E_a), and dihedral angle torsion (E_t) terms. Nonbond interaction is the van der Waals (E_{vdw}) potential. Each term is defined in the following equations:

TABLE I. Potential function parameters.

Parameter	Value
K_b	700 (kcal/mol)/Å^2
R_e	1.53 Å
K_θ	100 (kcal/mol)/rad^2
Θ_0	109.47°
V	2.0 kcal/mol
ϕ_0	180°

$$E_b = \tfrac{1}{2} K_b (R - R_e)^2, \tag{1}$$

$$E_a = \tfrac{1}{2} K_\theta (\Theta - \Theta_0)^2, \tag{2}$$

$$E_t = \tfrac{1}{2} V\{1 - \cos[n(\phi - \phi_0)]\}, \tag{3}$$

$$E_{vdw} = D_0 \left\{ \left[\frac{R_0}{R}\right]^{12} - 2\left[\frac{R_0}{R}\right]^{6} \right\}. \tag{4}$$

K_b and K_θ are valence force constants for a single bond and for all angle bends. R is the bond distance, Θ is the angle bend between two bonds, and ϕ is the dihedral angle. R_e, Θ_0, and ϕ_0 give potential minima. V is the total rotational barrier and $n=3$ is the periodicity of the potential, that is the number of potential local minima.

The van der Waals interactions between atoms separated by more than three bonds are given according to Lennard-Jones 12-6 potential. The length R_0 is the van der Waals bond length (Å), and the coefficient D_0 is the van der Waals well depth (kcal/mol). For two different kinds of atoms, these values are calculated by $(R_0)_{ij} = 1/2((R_0)_{ii} + (R_0)_{jj})$ and $(D_0)_{ij} = \sqrt{(D_0)_{ii}(D_0)_{jj}}$.

Nonbond interactions are handled by the spline switching method in which on–off parameters are defined and nonbond interactions are attenuated smoothly by a spline function between them. In this work, on–off parameters are 10.0 Å and 10.5 Å, respectively; nonbond interactions are considered exactly within 10.0 Å and ignored beyond 10.5 Å.

C. Dynamics, initial conditions, and sample preparation

We used a program package CERIUS2 (Accelrys Inc., San Diego, California) in molecular modeling and molecular dynamics simulations. We use the Verlet's leapfrog algorithm to solve the equations of motion. The molecular dynamics simulations are carried out under constant temperature which is controlled by the Nosé–Hoover thermostat.[30,31] The integration time step and the relaxation time of heat bath are 1.0 fs and 0.1 ps, respectively.

At first, we constructed the model whose torsional angles are all-*trans* conformation. To start the dynamics, velocities are given according to the Maxwell–Boltzmann distribution at a specified temperature (800 K). Only during the first run, we save structures every 2 ps for the first 18 ps calculations, to prepare nine other samples whose coordinates are different for each other. At this stage, these samples are not folded or a globule, and thus they are totally different in shape far from equilibrium. Calculations over ten runs are performed at the temperature from 800 K to 50 K.

TABLE II. Masses and constants used for the van der Waals parameters. United atoms of sp^3 carbons are classified into C_33, C_32, and C_31 whose last character indicates the number of implicit hydrogen atoms. For example, C_33 is the united atom with three implicit hydrogens, that is an end atom.

	Mass (g/mol)	R_0 (Å)	D_0 (kcal/mol)
C_33	15	4.15	0.250
C_32	14	4.07	0.198
C_31	13	3.98	0.147

Simulations are carried out for durations up to 15 ns from 800 K to 50 K with a stepwise lowering of the temperature 50 K every interval of 1 ns; the data of the first 900 ps at each temperature are discarded for equilibration; in the last 100 ps, coordinates at every 10 ps (ten configurations) are used for analyses.

Our average $\langle A(T)\rangle$ of a physical quantity $A(T)$ is evaluated first by taking an average over ten configurations of a single run, and second by taking a further average over the ten starting structures described above. The error bar is estimated by the values of the ten starting structures.

III. STATE OF THE ISOLATED CHAIN

In this section, before embarking upon the Voronoi analysis, we take a look at the shape and the state of the isolated chain at various temperatures. The shape of isolated polymer is intriguing and has been investigated theoretically[32–35] and numerically for a variety of chains generated by means of Monte Carlo simulations.[36–40]

Let X be the radius of gyration tensor for each configuration of chains, which is a symmetric matrix with elements defined by

$$X_{\alpha,\beta}=\frac{1}{N}\sum_{i=1}^{N} s_{\alpha i}s_{\beta i} \quad \alpha,\beta=x,y,z, \tag{5}$$

where $s_{\alpha i}$ and $s_{\beta i}$ are the coordinates of a vector s_i from the center of gravity of the chain to an ith atom. Since rotationally invariant quantity is required, the matrix X is diagonalized to yield eigenvalues, L_1^2, L_2^2, and L_3^2, which are moments along the principal axes of the chain,[32] and then the radius of gyration is expressed as

$$S^2=\mathrm{tr}\,X=L_1^2+L_2^2+L_3^2. \tag{6}$$

The asphericity A defined by Rudnick and Gaspari[33] is given by

$$A=\frac{\|(L_1^2-L_2^2)^2+(L_2^2-L_3^2)^2+(L_3^2-L_1^2)^2\|}{2\|(L_1^2+L_2^2+L_1^2)^2\|}, \tag{7}$$

where $\|\cdots\|$ denotes an average for a single run. It provides a generalized quantitative measure of the departure from spherical symmetry of the whole shape of a polymer chain. The value of A varies as $0\leqslant A\leqslant 1$: $A=0$ corresponds to an exact sphere and $A=1$ represents an extremely aspherical rodlike shape.

We plot S^2 and A as functions of temperature in Figs. 2 and 3, respectively. The radius of gyration becomes shorter with decreasing temperature during the process of stepwise cooling run. The tendency is pronounced above 500 K and modest below 450 K. The asphericity decreases from 800 K to 500 K, while it appears to be an approximately constant value 0.016 below 450 K. The increase of the radius of gyration above 500 K corresponds to the deviation from a sphere.

The structure changes into a globule near 500 K. To show that the state in the low-temperature region is globular, we have checked the number distribution function $h(r)$ as a function of their distance from the center of gravity. Figure 4 illustrates an example at 300 K. The data can be fitted up to 15 Å with a squared function, we hence confirm the uniform bulk property. Beyond this bulk region, the function decreases because of the surface (and the asphericity). In the following section, we apply the Voronoi analysis to the low-temperature region where the chain forms a globular structure.

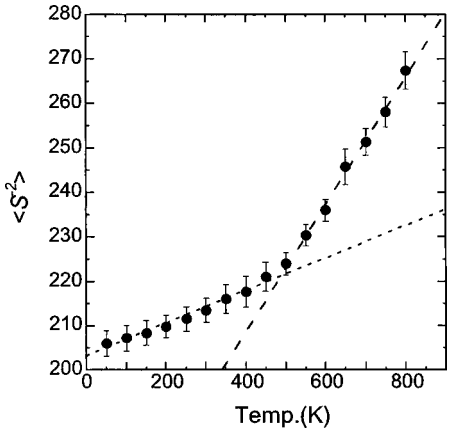

FIG. 2. Squared radius of gyration $\langle S^2\rangle$ against temperature. Error bars come from 10 starting structures. The coarse dashed and the fine dashed lines represent least-squares linear fittings to the data above 500 K and below 450 K, respectively.

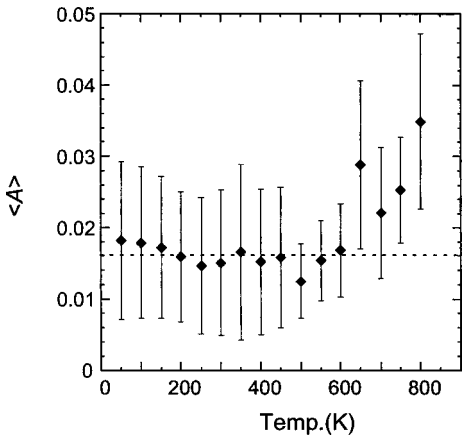

FIG. 3. Asphericity $\langle A\rangle$ against temperature. The asphericity at each temperature was averaged over ten configurations. The asphericity decreases upon lowering the temperature from 800 K to 500 K, while from 450 K to 200 K, it is approximately 0.016 indicated by the dashed line.

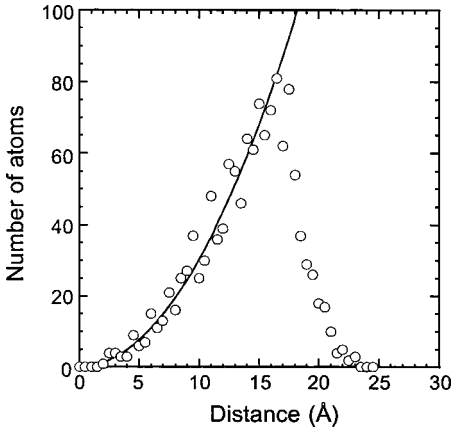

FIG. 4. Number distribution of atoms vs distance from the center of gravity (a snapshot at 300 K). The solid line is a fitting curve with a squared function meaning the bulk property.

IV. VORONOI ANALYSIS

A. Voronoi division

Several algorithms for Voronoi division have been proposed in the literature.[1–6] We will demonstrate that the traditional Voronoi analysis serves as a systematic approach to distinguish surface atoms from bulk atoms. To do so, we have modified Tanaka's algorithm.[5]

Given the positions of atoms, Voronoi division is uniquely defined as the closer regions of space to be constructed with bisecting planes between neighboring atoms. A two-dimensional analog is illustrated in Fig. 5. When an atom is in a bulk, the atom is surrounded by a convex polyhedron. The volume and the shape of each polyhedron give us the sufficient information to describe neighborhood associated with the central atom. When an atom is near a surface, the volume of the polyhedron is much larger than those of bulk atoms, or the polyhedron may fail to form, because surface atoms have fewer neighbors than bulk atoms, or no neighbors outward.

To judge whether bisecting planes form a closed polyhedron or an open structure, we take advantage of the Euler's relation. The Euler's relation for an arbitrary polyhedron is expressed as

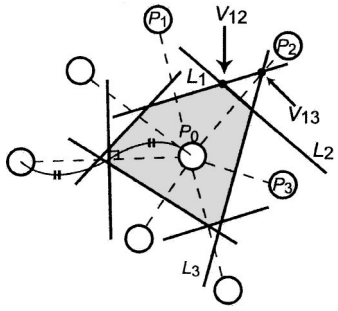

FIG. 5. Construction of a two-dimensional Voronoi polygon. By bisecting perpendicularly a line P_0P_i, a bisecting line L_i is generated. An intersection V_{ij} of two bisecting lines (L_i and L_j) is a trial vertex of the polygon associated with P_0. If V_{ij} lies inside all lines L_i, it becomes a vertex of the polygon, otherwise it is discarded: For example, V_{12} is a vertex and V_{13} is not.

$$v-e+f=2, \tag{8}$$

where v, e, and f are the numbers of vertices, edges, and faces, respectively. If the equation is satisfied for a set of these three numbers for an atom, we then calculate the volume. Otherwise, we assume that the region is open, and set the volume of the Voronoi polyhedron infinite.

The procedure for the analysis is as follows: The first step is the construction of a Voronoi polyhedron (1–5). The second step is to test whether or not the Euler's relation is fulfilled (6 and 7). The last step is the calculation of the volume. Details of each procedure are given below.

(1) Select atoms $P_i\,(i=1,2,3,...,M)$ within the sphere of radius $r_0=8$ Å centered at a central atom P_0. (The radius r_0 has been chosen by the economical reason in computation, and we have checked that the choice has no influence on the volume of any polyhedron.)
(2) Generate M perpendicularly bisecting planes between P_0 and $P_i\,(i=1,2,3,...,M)$.
(3) Select three arbitrary planes out of M bisecting planes, and find an intersection of these planes. The point is a trial vertex of the polyhedron.
(4) Check whether the trial vertex is placed inside all M planes, or not. If so, the vertex becomes a valid vertex of the polyhedron. To check, we have used the inner product of normal vector of a bisecting plane and the vector between the trail vertex and an arbitrary point in the bisecting plane.
(5) Repeat the procedures (3 and 4) for all combinations of three planes out of M, and find all vertices of the Voronoi polyhedron surrounding P_0.
(6) In practice, for every vertex of the polyhedron, a set of triplets (j, k, and l) indicating bisecting planes is assigned. Using the indices, we have computed the numbers of faces and edges of the polyhedron.
(7) Check whether or not the Euler's relation is satisfied. If not, the volume is assumed to be infinite.

Figure 6 displays some examples of Voronoi polyhedra: [Fig. 6(a)] An open polyhedron of $1/V=0$ at the surface of the globule and [Fig. 6(b)] a rodlike polyhedron of $1/V\approx 0$ near the surface. In the bulk, [Fig. 6(c)] an end atom, [Fig. 6(d)] an internal atom, and [Fig. 6(e)] a junction atom being more like a sphere are displayed.

B. Distribution of the inverse volume of polyhedra

Since the volume of polyhedra extends to infinity, we depict histograms as a function of the inverse of volume. Figures 7 and 8(a)–8(c) correspond to all atoms, end atoms, internal atoms, and junction atoms, respectively. These histograms of Figs. 7, 8(a), and 8(b) are flat around $1/V=0.02\,\text{Å}^{-3}$, and then increases as $1/V$ approaches 0. At $1/V=0$, there are exceptional peaks, corresponding to open polyhedra as shown in Fig. 6(a).

Paying attention to end atoms [Fig. 8(a)] whose peak position is smaller than the other, we assign atoms whose inverse volume is smaller than 0.02 Å^{-3} to surface atoms and other atoms to bulk atoms. See different viewpoints of the globule shown in Fig. 9. Surface atoms designated by the

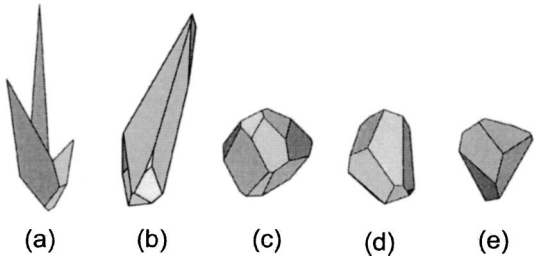

FIG. 6. Voronoi polyhedra. The shape of polyhedra becomes more prolate with decreasing $1/V$. (a) Open polyhedron ($1/V=0$). (b) Polyhedron ($1/V=0.013$ Å^{-3}). (c) Polyhedron ($1/V=0.032$ Å^{-3}). (d) Polyhedron ($1/V=0.053$ Å^{-3}). (e) Polyhedron ($1/V=0.080$ Å^{-3}). (a) and (b) are at the surface of the globule corresponding to Fig. 7 area $1/V<0.02$ Å^{-3}. (c), (d), and (e) correspond to I, II, and III in Fig. 7, respectively.

above definition are indicated by dark gray. One can notice that the circumference of the globule is occupied by dark gray atoms. Therefore, we think that the definition is reasonable.

For bulk atoms, as is seen in the peak shift in sequential Figs. 8(a)–8(c), the volume of a polyhedron has clear dependence upon the number of bonds; the volume becomes smaller with increasing number of bonds. The volume of polyhedra for ends is larger than that for internal atoms and junction atoms. From Fig. 8(c), it is evident that peak III in Fig. 7 is attributed to junction atoms, while the peak in Fig. 8(a) is not clearly seen in the left-hand side envelope of the peak in Fig. 7.

C. Temperature effect on the distribution

The distributions of $1/V$ for all atoms at various temperatures are shown in Fig. 10. With increasing temperature, the distribution for bulk atoms becomes broader due to volume fluctuations and the peak shifts to smaller values due to thermal expansions. The bulk atom regions for ends I and for junction atom III exhibit the same tendency as shown in Fig. 11. In the surface atom regions, the temperature effect seems to be little, in contrast to what occurs in the bulk atom regions.

To see the temperature dependence of thermal expansion and volume fluctuations more clearly, assuming the distributions I, II, and III in Figs. 10 and 11 to be Gaussian, we have obtained the mean values μ and the standard deviations σ

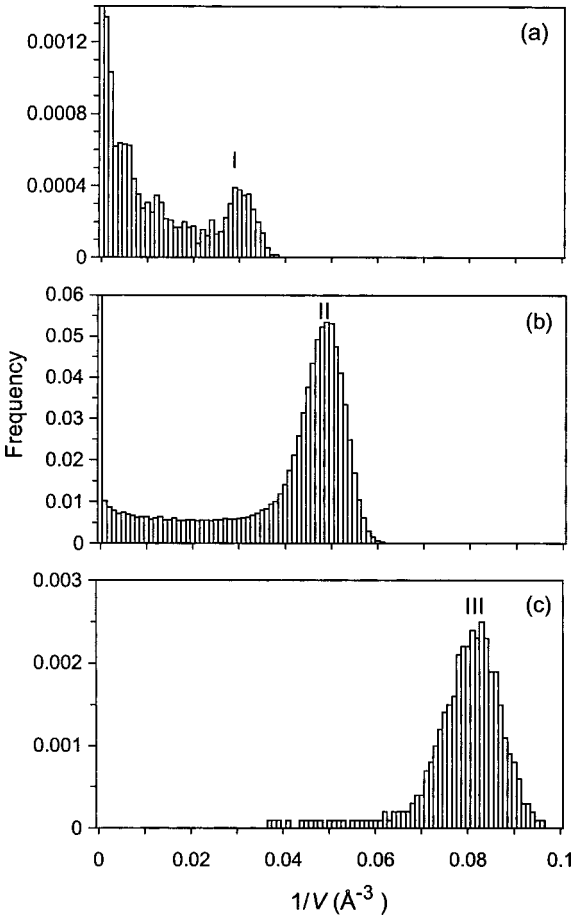

FIG. 8. Histograms of the frequency distribution of the inverse polyhedron volume $1/V$ at 300 K for three types of atoms. (a) End atoms. Peak I near $1/V=0.03$ corresponds to shoulder I in Fig. 7. (b) Internal atoms. Peak II at $1/V=0.05$ corresponds to peak II in Fig. 7. (c) Junction atoms. Peak III corresponds to peak III in Fig. 7. The frequencies at $1/V=0$ in (a) and (b) are 0.028 and 0.074, respectively.

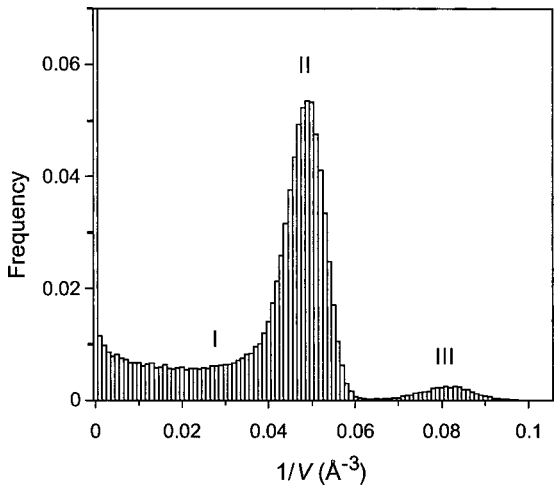

FIG. 7. Histogram of the frequency distribution of the inverse polyhedron volume $1/V$ at 300 K for all atoms. For Figs. 7, 8, 11, and 12, by taking two step averages of 100 configurations (10 configurations times 10 starting structures), smooth histograms have been obtained. The histogram interval is 0.001 Å^{-3}. There is an exceptional peak at $1/V=0$, corresponding to open polyhedra. I indicates a small shoulder near $1/V=0.03$ corresponding to a visible peak in Fig. 8(a). Peak II corresponds to a Gaussian-type peak at $1/V=0.05$. Peak III corresponds to a small peak near $1/V=0.08$.

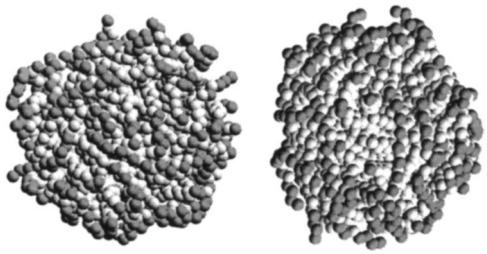

FIG. 9. Surface atoms defined by $1/V<0.02$ Å^{-3} are indicated by dark gray spheres. Notice that the circumference of the two-dimensional visualization is occupied by the dark gray atoms; the definition works.

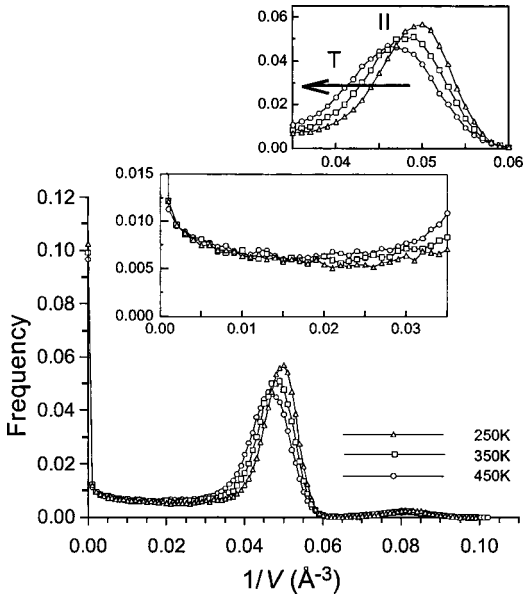

FIG. 10. Distribution of $1/V$ for all atoms at 250 K, 350 K, and 450 K. With increasing temperature, the distribution of bulk atoms denoted by II becomes broader and the peak shifts to smaller $1/V$, while the influence of temperature on the distribution in a flat region around $1/V=0.02$ is little.

through curve fitting. Although envelopes for the smaller $1/V$ values are almost constant and not the Gaussian distributions, we ignore the envelopes.

The meaning of these two values μ and σ are evident, since when we define

$$\mu=\left\langle\frac{1}{V}\right\rangle, \quad \sigma^2=\left\langle\frac{1}{V^2}\right\rangle-\mu^2, \tag{9}$$

$$\tilde{V}=\langle V\rangle, \quad \sigma_V^2=\langle V^2\rangle-\tilde{V}^2, \tag{10}$$

a brief calculation yields

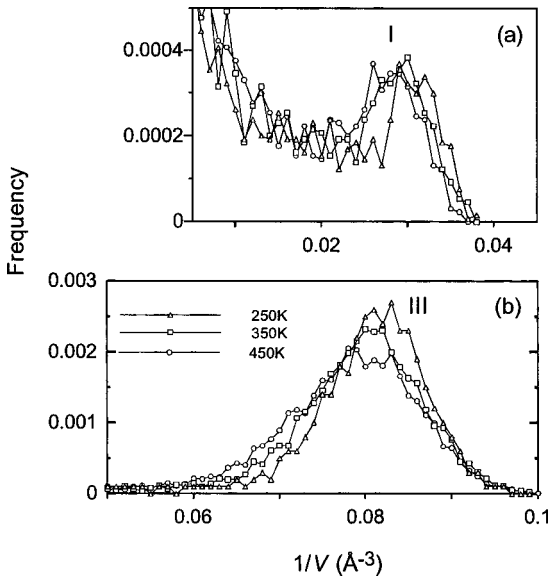

FIG. 11. Temperature effect on the distributions of $1/V$. (a) and (b) show the distribution of only end atoms and only junction atoms, respectively. Temperature effects on these distributions of I and III are the same as the distribution of II.

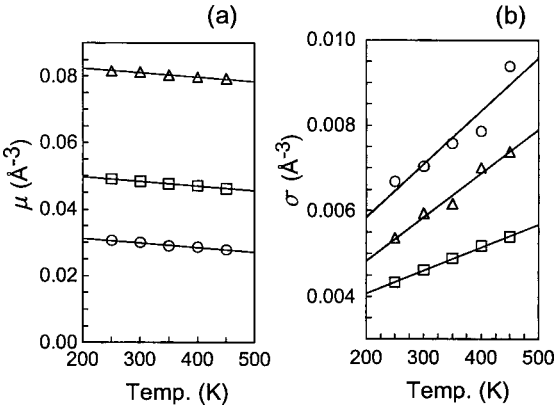

FIG. 12. Mean value μ (a) and standard deviation σ (b) of $1/V$ for bulk atoms plotted against temperature. With increasing temperature, polyhedron volume becomes larger and fluctuates more vigorously. ○: End atoms, □: Internal atoms, and △: Junction atoms.

$$\mu=\frac{1}{\tilde{V}}+\frac{\sigma_V^2}{\tilde{V}^3}-O\left(\frac{1}{\tilde{V}^4}\right), \tag{11}$$

$$\sigma^2=\frac{\sigma_V^2}{\tilde{V}^4}+O\left(\frac{1}{\tilde{V}^5}\right). \tag{12}$$

Therefore, we reasonably assume that

$$\mu\approx\frac{1}{\tilde{V}}, \quad \sigma\approx\frac{\sigma_V}{\tilde{V}^2}, \quad \frac{\sigma}{\mu}\approx\frac{\sigma_V}{\tilde{V}}. \tag{13}$$

The temperature dependence of μ and σ is plotted in Fig. 12. It is evident that the polyhedron volume of each atom and the fluctuations become larger with increasing temperature.

In addition, the dimensionless value $\mu(T)/\mu(T=250\,\mathrm{K})$ against temperature is plotted in Fig. 13. Notice that the slope $-\Delta\mu/(\mu\Delta T)$ corresponds to the thermal expansion coefficient:

$$\kappa=-\frac{1}{1/V}\left(\frac{\partial(1/V)}{\partial T}\right)_p=-V\left(\frac{\partial S}{\partial p}\right)_T. \tag{14}$$

Based on Fig. 13, we conclude that the Voronoi volume concerning ends exhibits the largest thermal expansion and that for junction atoms shows the smallest thermal expansion.

D. Surface segregation of chain ends

In Fig. 14, end atoms are depicted by dark gray spheres. At the surface of the globule, we can see a number of chain ends and the side chain ends. In fact, from 50 K to 450 K, surface atoms are 24% of all atoms, while ends at the surface are 91% of all ends. The temperature dependence has been found to be quite small, because in the cooling run the vast change of conformations does not happen. The data were averaged over ten samples.

Two reasons have been argued in literature for why ends favor surfaces. On the one hand, a purely entropic reason has been argued that ends do not suffer from the loss of conformational entropy due to the imposed reflection at a surface,[13,14] therefore the segregation arises [Fig. 15(a)]. One the other hand, there is a free volume contribution to reduce

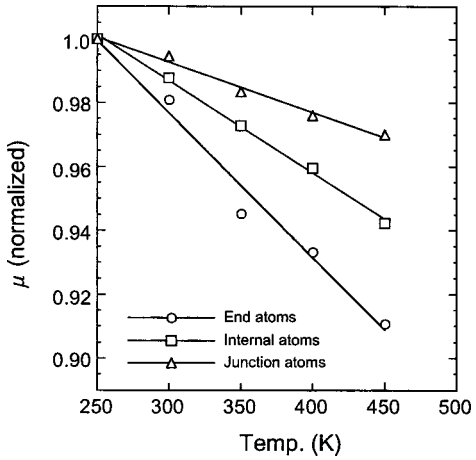

FIG. 13. Normalized mean value of $1/V\ \mu/\mu(250\ \mathrm{K})$ against temperature for bulk atoms. Slopes correspond to the "microscopic" thermal expansion coefficients. The slope for end atoms is the steepest downward implying that the microscopic thermal expansion for the ends are the largest.

the surface free energy, namely, entropy gain by using larger free volume[12] associated with ends [Fig. 15(b)].

It is very hard to discriminate these two mechanisms, because the energy scale is the same, however, our elucidation suggests that the end localization to the surface arises from the free volume contribution. Since the boundary of our chain is not a hard wall but a free surface, ends take advantage of free volume.

Furthermore, not only end atoms appear on the surface, but also ends pull up some connected atoms to gain entropy in the free space regardless of energy reduction. About 60% of the next to end are surface atoms as shown in Fig. 16. As expected, the closer to the end, the higher the probability of the surface atoms. We call this the *pull mechanism* [Fig. 15(c)]. See some popped end parts in Fig. 14. This mechanism is the extension of the free volume mechanism and the force for pulling is the entropic force. If the zigzag move due to covalent bonding in Fig. 16 is ignored, the percentage becomes smaller as atoms get closer to junctions.

E. Shapes of Voronoi polyhedra

Below, we describe detailed shape analysis at 300 K.

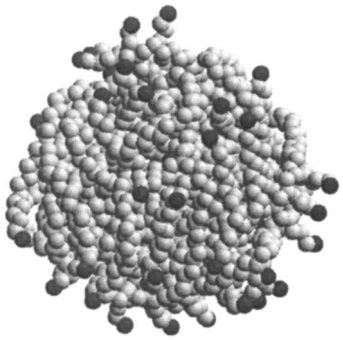

FIG. 14. Instantaneous snapshot at 300 K. 52 end atoms are represented by dark gray spheres. It reveals a considerable degree of roughness at the surface and shows that ends are favorably near the surface.

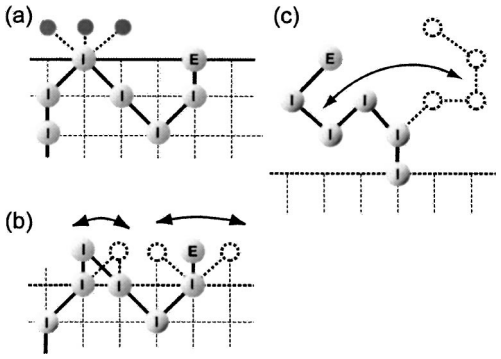

FIG. 15. Schematic illustration of entropic contributions to the surface free energy. (a) No-reflection mechanism: There is entropy loss for internal atoms (I) by imposed reflection at a surface, while there is no entropy loss for ends (E). Black positions are disallowed positions for I's. (b) Free volume mechanism: There is entropy gain by larger free volume. E's are less restrictive and thus gain more entropy than I's. (c) Pull mechanism: E's pull up connected atoms by entropic force. This mechanism is the extension of (b).

1. Shape factors

In analogy with the method described in the previous section, we clarify whether a polyhedron is oblate (disklike) or prolate (rodlike). The tensor X in Eq. (5) is now calculated by using coordinates of vertices of a polyhedron and is diagonalized to yield eigenvalues L_1^2, L_2^2, and L_3^2 ($L_1^2 \leqslant L_2^2 \leqslant L_3^2$) which are principal moments. They are divided by S^2 in order to compare configurations of the different sizes. We then obtain the dimensionless shape factors[36] g_n:

$$g_n = \frac{L_n^2}{S^2}, \quad n = 1,2,3, \tag{15}$$

where $S^2 = \mathrm{tr}\, X = L_1^2 + L_2^2 + L_3^2$.

A sphere is characterized by

$$g_1 = g_2 = g_3 = \tfrac{1}{3},$$

while for an extremely prolate (rodlike) shape, they become

$$g_1 = g_2 \approx 0, \quad g_3 \approx 1,$$

and for an extremely oblate (disklike) shape, they are

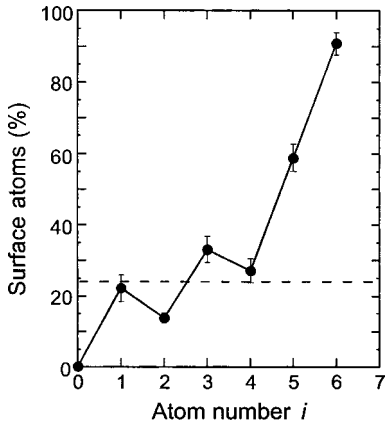

FIG. 16. Probability of surface atoms at 300 K vs the number from a junction atom in a side chain: $i=0$, junction; $i=6$, end. The dashed line indicates the probability of surface atoms for all atoms, 23.9%. Error bars come from ten starting structures.

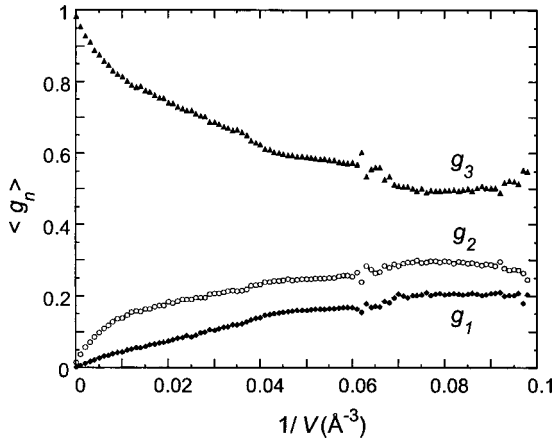

FIG. 17. Shape factors of a Voronoi polyhedron vs $1/V$ at 300 K. The range of $1/V$ was divided into $\Delta 1/V = 0.001$ Å^{-3} intervals. For bulk atoms, the shape of polyhedra is prolate, because $\langle g_3 \rangle$ is larger than the others. At the surface, the shape is more prolate, because $\langle g_1 \rangle$ and $\langle g_2 \rangle$ approach 0 and $\langle g_3 \rangle$ approaches 1 as the volume of a polyhedron becomes large.

$$g_1 \approx 0, \quad g_2 = g_3 \approx 0.5.$$

Figure 17 displays the plot of the shape factors against $1/V$. The plot illustrates basically that

$$\langle g_1 \rangle \sim \langle g_2 \rangle < \langle g_3 \rangle,$$

implying that the shape of a polyhedron is prolate, with a little asymmetry of $\langle g_1 \rangle$ and $\langle g_2 \rangle$.

As the volume becomes larger, two factors $\langle g_1 \rangle$ and $\langle g_2 \rangle$ approach zero, while $\langle g_3 \rangle$ approaches 1.0, indicating that the shape of a polyhedron for surface atoms whose volume is large, is prolate or rodlike.

The curves in Fig. 17 are not smooth. To look into bulk atoms more carefully, averaged shape factors for each kind of atoms in each peak region between $\mu \pm \sigma$ in Figs. 8(a)–8(c) are listed in Table III. From Table III, we find that polyhedra containing internal atoms are more prolate compared to other types of atoms.

2. Bonding faces

We have seen that the polyhedra containing bulk atoms are not spherical. To clarify the reason, we consider the characteristic feature of polymers: In space, there are not only atoms but also covalent bonds between atoms. We call the face of a Voronoi polyhedron that bisects a covalent bond, a *bonding face*.

For an internal atom in the united-atom model, there are two bonding faces, which are the closest (or the second closest due to thermal vibrations) to the atom. On the other hand, for an end atom, the closest plane is the only one bonding face and the second closest face is bisected with the next neighbor atom from the end atom. The angles between these two faces are about 70° for an internal atom and 145° for an end (see Fig. 18). In the case of the internal atom, the atom is well surrounded by bonding faces due to the acute angle, while in the case of ends, the front space is relatively open.

TABLE III. Averaged shape factors $\langle g_i \rangle$ of polyhedra for typical bulk atoms in peak regions between $\mu \pm \sigma$ in Fig. 8.

Atom	$\langle g_1 \rangle$	$\langle g_2 \rangle$	$\langle g_3 \rangle$	$\mu - \sigma$	$\mu + \sigma$	in Å^{-3}
End	0.181	0.332	0.487	0.023	0.037	
Internal	0.160	0.248	0.592	0.044	0.053	
Junction	0.207	0.296	0.497	0.075	0.087	

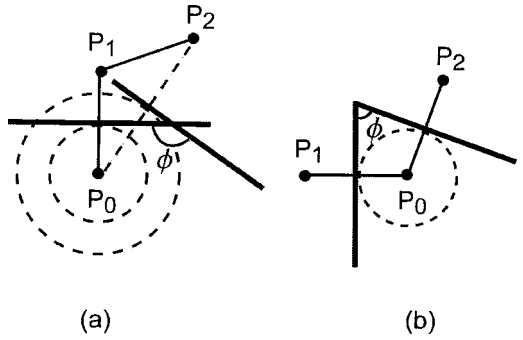

FIG. 18. Relation between a central atom P_0 and the closest neighboring atom P_1 and the next closer atom P_2. They are along the chain. (a) P_0: end atom, (b) P_0: internal atom. The angle ϕ between the bonding face and the second closest face is 145° in (a) and that between two bonding faces is 70° in (b).

Correspondingly, the number of faces per polyhedron reflects the circumstance, narrow or open space caused by bonding faces. Here, we consider typical bulk atoms in peak regions between $\mu \pm \sigma$ in Figs. 8(a)–8(c). Figure 19 plots the distribution of the number of faces per polyhedron. The average number of faces per polyhedron is 11.0, 15.3, and 19.2 for junction atoms, internal atoms, and end atoms, respectively.

Since the distance to a bonding face is the closest, the area of the bonding face becomes the largest. As shown in Fig. 20, the sum of areas of two bonding faces is 38.2% of the total surface area of a polyhedron for internal atoms, which is notably large; for ends that of the bonding and the next nearest face is 26.6%.

Furthermore, there is a strong orientational correlation between the principal axis associated with the largest eigenvalue L_3^2 (or g_3) and the edge where two bonding faces meet.

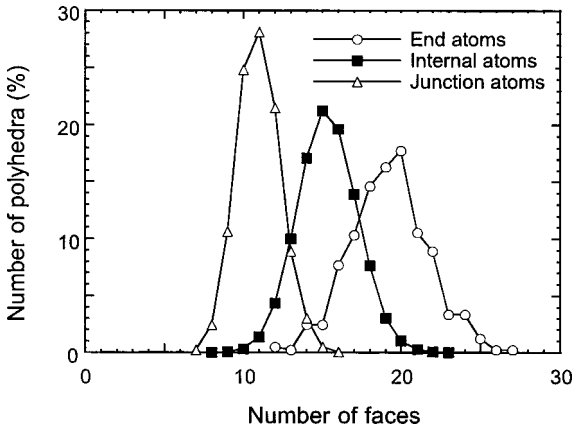

FIG. 19. Histogram for the number of faces per polyhedron for typical bulk atoms at 300 K. The more the number of bonds, the fewer the number of faces of a polyhedron.

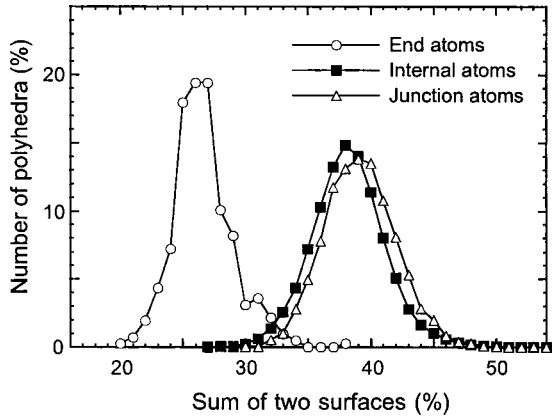

FIG. 20. Proportion of the sum of two areas to the total surface area of a polyhedron for typical bulk atoms at 300 K. For internal and junction atoms, two areas consist of the two bonding faces. For ends, two areas consist of the bonding face and the face formed by the next nearest atom. The sum of only two bonding face areas out of 15.3 faces (average) amounts to 38.2% of the total area for internal atoms.

Figure 21 shows that the principal direction for g_3 and that of the edge are nearly parallel.

To get a quantitative estimation of the orientational correlation, we use an order parameter[41] Q defined by

$$Q = \tfrac{1}{2}\{3\langle\cos^2\theta\rangle - 1\}, \tag{16}$$

where θ is the angle between the principal axis and the edge as shown in Fig. 21. For a perfect correlation, Q becomes 1, implying always parallel between the principal axis and the edge for each polyhedron, and for uniformly randomly orientations it takes 0. In our simulations, we have obtained $Q=0.970$ for internal atoms. For ends, by taking a bonding face and the next nearest one, $Q=0.738$.

V. CONCLUSION

The Voronoi analysis is of greatest utility for investigating the spatial structure of polymeric materials. We have seen from the $1/V$ histograms that the Voronoi polyhedron volume is related to the topology of atoms: The volume associated with end atoms is larger than that associated with internal and junction atoms. Clearly, the motion of internal atoms is restricted by the connection on both sides, while ends are less restrictive[42] and move easily. The largest volume and the prominent microscopic thermal expansion of ends reflect the highest mobility. We note here that the capability to define microscopic (local) thermal expansion is the advantage of the Voronoi analysis.

The $1/V$ histogram is also useful to distinguish between surface and bulk parts. Then, we have obtained remarkable evidence that end atoms favor the surface. It is quite reasonable that side chain ends are usually functional parts, whose structure takes advantage of the mobility of the ends, leading to the increase of reactivity at a surface and in a bulk region.

In terms of shape factors that contain information of three principal directions representing whether the shape of Voronoi polyhedra is prolate or oblate, we have found that the shape of Voronoi polyhedra is prolate even in the bulk region and become more prolate near the surface region, thereby they finally break up and become open polyhedra. The factors provide more information than the one parameter that has been used in the preceding studies.[8,9]

We have introduced the concept of bonding faces that allow us to understand why the polyhedra of internal atoms are prolate. We have evaluated that although the number of faces per polyhedron is 15.3, two bonding faces occupy close to 40% of the total surface area of a polyhedron. In addition, it is intriguing that the principal direction corresponding to the largest shape factor, i.e., the direction of a rod is parallel to the edge between two bonding faces. Therefore, we can say that two bonding faces play a significant role to determine the shape of a polyhedron.

In contrast to Ref. 9, pointing out the close relation to random packings of hard spheres, we emphasize the importance of bonding faces which represent the characteristic feature of the Voronoi space division of covalent bonded polymers, namely, the very existence of bonds; that is why a material is polymeric.

Finally, we anticipate that the Voronoi analysis will shed light on the understanding of microscopic structures of polymers concerning physical properties, chemical reactivity, and biological functions. The notion of microscopic thermal expansion and that of bonding faces are such insights which the Voronoi analysis of polymers allows us to put forward.

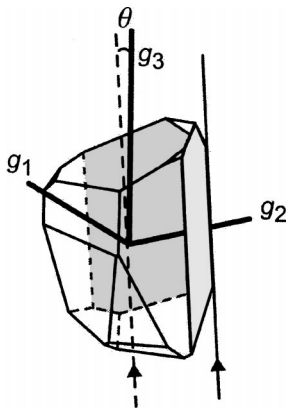

FIG. 21. The relation between a polyhedron shape and the principal axes of the shape factors. θ is the angle between the principal axis of g_3 and the edge between bonding faces.

ACKNOWLEDGMENTS

This work was supported by a special research grant of the University of the Air. The authors are grateful to Professor Susumu Fujiwara for helpful discussions and Norishige Matsuzaki and Kotaro Nomura for technical assistance.

[1] J. L. Finney, Proc. R. Soc. London, Ser. A **319**, 479 (1970); J. Comput. Phys. **32**, 137 (1979).
[2] M. R. Hoare, J. Non-Cryst. Solids **31**, 157 (1978).
[3] W. Brostow, J.-P. Dussault, and B. L. Fox, J. Comput. Phys. **29**, 81 (1978).
[4] M. Tanemura, T. Ogawa, and N. Ogita, J. Comput. Phys. **51**, 191 (1983).
[5] M. Tanaka, J. Phys. Soc. Jpn. **55**, 3108 (1986).
[6] N. N. Medvedev, J. Comput. Phys. **67**, 223 (1986).
[7] Voronoi analysis has been used not only in condensed matter physics, but also in a wide variety of fields such as mathematics, computational geometry, biology, and city planning, which are inherently geometrical. See, for example, F. Aurenhammer, ACM Comput. Surv. **23**, 345 (1991), and references therein.

[8] D. Rigby and R. J. Roe, Macromolecules **23**, 5312 (1990).
[9] A. Soyer, J. Chomilier, J.-P. Mornon, R. Jullien, and J.-F. Sadoc, Phys. Rev. Lett. **85**, 3532 (2000).
[10] T. G. Fox and P. J. Flory, J. Appl. Phys. **21**, 581 (1950).
[11] B. B. Sauer and G. T. Dee, Macromolecules **24**, 2124 (1991).
[12] G. T. Dee and B. B. Sauer, J. Colloid Interface Sci. **152**, 85 (1992); B. B. Sauer and G. T. Dee, *ibid.* **162**, 25 (1994).
[13] P.-G. de Gennes, C. R. Acad. Sci. (Paris) **307**, 1841 (1988); See also, *Simple Views on Condensed Matter: Expanded Edition* (World Scientific, Singapore, 1998), p. 405.
[14] A. Hariharan, S. K. Kumar, and T. P. Russell, Macromolecules **23**, 3584 (1990).
[15] R. A. L. Jones and R. W. Richards, *Polymers at Surfaces and Interfaces* (Cambridge University Press, Cambridge, UK, 1999).
[16] S. K. Kumar, M. Vacatello, and D. Y. Yoon, J. Chem. Phys. **89**, 5206 (1988); Macromolecules **23**, 2189 (1990).
[17] D. N. Theodorou, Macromolecules **22**, 4578 (1989).
[18] I. Bitsanis and G. Hadziioannou, J. Chem. Phys. **92**, 3827 (1990).
[19] A. Yethiraj and C. K. Hall, Macromolecules **23**, 1865 (1990).
[20] J. G. Harris, J. Phys. Chem. **96**, 5077 (1992).
[21] R. G. Winkler, T. Matsuda, and D. Y. Yoon, J. Chem. Phys. **98**, 729 (1993).
[22] A. M. Mayes, Macromolecules **27**, 3114 (1994).
[23] D. T. Wu, G. H. Fredrickson, J.-P. Carton, A. Ajdari, and L. Leibler, J. Polym. Sci., Part B: Polym. Phys. **33**, 2373 (1995).
[24] S. Affrossman, M. Hartshorne, R. Jerome, R. A. Pethrick, S. Petitjean, and M. Rei Vilar, Macromolecules **26**, 6251 (1993).
[25] W. Zhao, X. Zhao, M. H. Rafailovich *et al.*, Macromolecules **26**, 561 (1993).
[26] A. M. Botelho do Rego, J. D. Lopes da Silva, M. Rei Vilar, M. Schott, S. Petitjean, and R. Jérôme, Macromolecules **26**, 4986 (1993).
[27] T. Kajiyama, K. Tanaka, and A. Takahara, Macromolecules **30**, 280 (1997).
[28] K. Tanaka, A. Takahara, and T. Kajiyama, Macromolecules **33**, 7588 (2000).
[29] S. L. Mayo, B. D. Olafson, and W. A. Goddard, J. Phys. Chem. **94**, 8897 (1990).
[30] W. G. Hoover, Phys. Rev. A **31**, 1695 (1985).
[31] S. Nosé, J. Chem. Phys. **81**, 511 (1984).
[32] K. Šolc and W. H. Stockmayer, J. Chem. Phys. **54**, 2756 (1971); K. Šolc, *ibid.* **55**, 335 (1971).
[33] J. Rudnick and G. Gaspari, J. Phys. A **19**, L191 (1986).
[34] J. A. Aronovitz and D. R. Nelson, J. Phys. (France) **47**, 1445 (1986).
[35] H. W. Diehl and E. Eisenriegler, J. Phys. A **22**, L87 (1989).
[36] J. Mazur, C. M. Guttman, and F. L. McCrackin, Macromolecules **6**, 872 (1973).
[37] M. Bishop, J. H. R. Clarke, A. Rey, and J. J. Freire, J. Chem. Phys. **94**, 4009 (1991).
[38] G. Zifferer, J. Chem. Phys. **109**, 3691 (1998).
[39] M. Triantafillou and R. D. Kamien, Phys. Rev. E **59**, 5621 (1999).
[40] V. A. Ivanov, M. R. Stukan, V. V. Vasilevskaya, W. Paul, and K. Binder, Macromol. Theory Simul. **9**, 488 (2000).
[41] P.-G. de Gennes and J. Prost, *The Physics of Liquid Crystals* (Oxford University Press, New York, 1993), p. 41.
[42] J. Horinaka, M. Maruta, S. Ito, and M. Yamamoto, Macromolecules **32**, 1134 (1999).